X-ray spectrum of a pinned charge density wave

Alberto Rosso and Thierry Giamarchi

Université de Genève, DPMC, 24 Quai Ernest Ansermet, CH-1211 Genève 4, Switzerland

(Received 4 June 2004; published 14 December 2004)

We calculate the x-ray diffraction spectrum produced by a pinned charge density wave (CDW). The signature of the presence of a CDW consists of two satellite peaks, asymmetric as a consequence of disorder. The shape and the intensity of these peaks are determined in the case of a collective weak pinning using the variational method. We predict divergent asymmetric peaks, revealing the presence of a Bragg glass phase. We deal also with the long range Coulomb interactions, concluding that both peak divergence and anisotropy are enhanced. Finally we discuss how to detect experimentally the Bragg glass phase in the view of the role played by the finite resolution of measurements.

I. INTRODUCTION

The study of disordered elastic objects sheds light on the physics of a wide range of systems. A first class of systems is accurately modeled by elastic manifolds in the presence of randomness; significant examples include domain walls in magnetic[1] or ferroelectric[2] materials, contact lines of liquid menisci on a rough substrate,[3] and propagating cracks in solids.[4] A second class of disordered elastic systems is given by periodic structures such as charge density waves (CDWs),[5] vortex flux lines in type-II superconductors[6] and Wigner crystals.[7] It was recently shown that periodic systems have unique properties, quite different from the ones of the interfaces. In fact, if topological defects (i.e., dislocations, etc.) in the crystal are excluded, displacements can grow only logarithmically,[8–10] in contrast with the power-law growth of interfaces. The positional order is only algebraically destroyed,[10,11] leading to divergent Bragg peaks and a nearly perfect crystal state. Quite remarkably, it was shown that for weak disorder this solution is *stable* to the proliferation of topological defects, and thus that a thermodynamically stable phase having both glassy properties and quasi-long-range positional order exists.[11] This phase, nicknamed Bragg glass, has prompted many further analytical and experimental studies (see, e.g., Refs. 12 and 13 for reviews and further references). Although its existence can be tested indirectly by the consequences on the phase diagram of vortex flux lines, the most direct proof is to measure the predicted algebraic decay of the positional order. Such a measurement can be done by means of diffraction experiments, using either neutrons or x rays. Neutron diffraction experiments have recently provided unambiguous evidence[14] of the existence of the Bragg glass phase for vortex lattices.

Another periodic system in which one can expect a Bragg glass to occur are CDWs,[5] where the electronic density shows a sinusoidal modulation. As a consequence of the electron–phonon interaction, this modulation generates a permanent distortion of the underlying lattice. This distortion can be revealed thanks to x-ray measurements: in fact, the corresponding x-ray spectrum presents satellite peaks around each principal Bragg peak. These satellites contain information concerning the positional order of the CDW. In particular, we are interested in the detection of effects due to

disorder.[15] The x-ray experimental resolution is in principle much higher than the one that can be achieved by neutrons for vortex lattices, consequently CDW systems should be prime candidates for studying the detailed nature of a Bragg glass state.[16] It should in particular be possible to *directly* probe the power law nature of the Bragg peaks predicted for a Bragg glass. However, compared to the case of vortex lattices the interpretation of the spectrum is much more complicated for two main reasons: (i) the phase of the CDW is the object described by an elastic energy, whereas the x rays probe the displacements of the atoms in the crystal lattice (essentially a cosine of the phase); (ii) since the impurities substitute for some atoms of the crystal, the very presence of the impurities changes the x-ray spectrum. This gives rise to nontrivial terms of interference between disorder and atomic displacements.[16,17] It is thus necessary to make a detailed theoretical analysis of the diffraction due to a pinned CDW.

In the past, the study of the spectrum has been carried out only either for strong pinning or at high temperatures.[16–19] In this paper we focus on the low temperature limit, where a well formed CDW exists, and on weak disorder, for which one expects to be in the Bragg glass regime. Both the short and long range screening of the Coulomb interactions are considered. We show that in both cases the diffraction spectrum consists of two asymmetric peaks. The peaks are power-law divergent, with a stronger anisotropic shape in the case of unscreened long-range Coulomb interaction. This finding is consistent with the Bragg glass behavior.[11] The asymmetry divergence follows a subdominant power-law as well, with an exponent that we determine. A short account of part of the results of this paper was published in Ref. 20.

In Sec. I we derive the model used to describe the interaction between the CDW and impurities. Two elastic limits are considered: if free electrons are present the elasticity has a simple short-range form, while, in the unscreened case, Coulomb interactions are responsible for a long range strongly anisotropic elastic term. In Sec. II we discuss the x-ray intensity spectrum behavior in presence of a pinned CDW. In particular, we derive the different contributions to the satellite peaks and we study their symmetry properties. In Sec. III we evaluate explicitly the different terms by means of the replica techniques. Section IV contains the physical discussion in view of all the results obtained in this paper.

The reader not interested in the details of calculations may move directly to this section skipping the previous one. Finally, in Appendix A we evaluate the triplet contribution and in Appendix B we calculate the function $[\sigma]$, used in Sec. IV.

II. THE MODEL

The system we have studied is a CDW in a three dimensional space. The electron density has the form:[21]

$$\rho(r) = \rho_0 + \frac{\rho_1 |\psi| Q^{-1}}{\pi} \nabla \phi(r) + \rho_1 |\psi| \cos[Qr + \phi(r)], \quad (1)$$

where a single sinusoidal deformation of modulation vector Q is considered and $\psi = |\psi| e^{i\phi}$ is the CDW order parameter normalized to unity at $T=0$. The first term of Eq. (1), ρ_0, is the average density. The second one corresponds to a density averaged at scales larger than Q^{-1}. This contribution, also called *forward scattering*, encompasses the local changes of the electron density related to the compression modes. The last term, also called backward scattering, describes the sinusoidal modulation at a scale of the order of Q^{-1}. We can neglect all contributions stemming from higher harmonic terms as they are known to be important only at very low temperature. The effective Hamiltonian can be obtained by a Ginzburg–Landau expansion of the order parameter

$$H = \int d^3 r \frac{1}{2} |\psi|^4 - a |\psi|^2 + \frac{b}{2} |\nabla \psi|^2, \quad (2)$$

where $a = (T_c - T)/T_c$ and b is a parameter whose value is defined by the microscopic theory. The configuration at minimum energy corresponds to $|\psi| = \sqrt{a}$ with the phase ϕ equal to a constant. Around this equilibrium solution, fluctuations involve both the amplitude and the phase of the order parameter. We remark that while the first ones are more expensive in terms of energy variations, due to the presence of the quadratic term, the second ones are massless. Following the model developed by Fukuyama-Lee-Rice (FLR),[15,22,23] we take into account only the phase fluctuations (i.e., we neglect amplitude fluctuations). The mass of these excitations, called phasons, turns out to be quite large, because it depends on the ionic mass via the electron–phonon interaction. For this reason, we can neglect in the Hamiltonian the kinetic term giving rise to quantum fluctuations. Within these hypotheses, the elastic Hamiltonian associated to the CDW reads

$$H_{el} = \int d^3 r \frac{c}{2} [\nabla \phi(r)]^2, \quad (3)$$

where $c = b|\psi|^2$ is the elastic constant. The thermal fluctuations of the phase, denoted as ϕ_T, are easily evaluated:

$$\phi_T^2 = 2\langle \phi^2(x) \rangle$$

$$= 2 \int \mathcal{D}\phi \phi^2 e^{-H/T} = 2T \int_{BZ} \frac{1}{cq^2} \sim \frac{QT}{\pi^2 c}. \quad (4)$$

The integral in q extends all over the Brillouin zone. In the low temperature regime, the fluctuations are thus small enough to guarantee the presence of an ordered phase. More-

over, we observe that the value of the integral (4) is related to the shortest length scale in the problem. Here we assume that this cutoff momentum, Λ, is given by the periodicity of the CDW ($\Lambda \sim Q$).[35]

The form of the Hamiltonian (3) is actually anisotropic along the Q direction. In fact, a compression along Q produces an increase of the electric charge density which yields an increase of the stiffness, whereas all distortions along the other two directions do not involve any change in electrostatic energy.

We evaluate the contribution of Coulomb interactions screened beyond the characteristic length λ. Without any loss of generality we assume $Q \| x$ and y is along one of the other two equivalent directions. The electrostatic energy takes the form:

$$U \propto \frac{1}{2V} \int d^3 r \, d^3 r' \, e^{-|r-r'|/\lambda} \frac{\rho(r)\rho(r')}{|r-r'|}. \quad (5)$$

The main contribution to the electrostatic energy comes from the variations of the electron density ρ, expressed by Eq. (1). Therefore, we restrict to consider only the forward scattering term:

$$U \propto \frac{\rho_1^2 |\psi|^2}{2\pi^2 Q^2 V} \int d^3 r \, d^3 r' \, e^{-|r-r'|/\lambda} \frac{\partial_x \phi(r) \partial_{x'} \phi(r')}{|r-r'|}$$

$$= \frac{\rho_1^2 |\psi|^2}{\pi Q^2} \int_{BZ} \frac{(q_x \lambda)^2}{1 + \lambda^2 q^2} |\phi(q)|^2. \quad (6)$$

This term introduces a q dispersion in the elastic constant

$$H_{el} = \int_{BZ} \left[c_1(q) q_x^2 + \frac{c}{2} q^2 \right] |\phi(q)|^2$$

$$c_1(q) \propto \frac{\lambda^2}{1 + q^2 \lambda^2}.$$

Two regimes can be identified as a function of the screening length λ. (i) In the first one, valid for λ not very large, we can neglect the dispersion in q and the resulting elasticity is short range. The effect of Coulomb interaction is an enhancement of the elastic constant along the x direction

$$H_{el} = \int dx \, d^2 y \left[\frac{c_1}{2} (\partial_x \phi)^2 + \frac{c}{2} (\partial_y \phi)^2 \right]. \quad (7)$$

By redefining the spatial variables, $x' = x/\sqrt{c_1}$ and $y' = y/\sqrt{c}$, with $c = (c_1 c^2)^{1/2}$, the Hamiltonian (7) can be finally turned into an isotropic form. (ii) The second regime is characterized by large values of λ. In this case, the electrostatic energy takes the form $U \sim \int_{BZ} (q_x^2/q^2) |\phi(q)|^2$, and consequently a long-range term appears in the elasticity:

$$H_{el} = \int \frac{dq_x}{2\pi} \frac{d^2 q}{(2\pi)^2} \left[\frac{c_1}{2} \frac{q_x^2}{q^2} + \frac{c}{2} q^2 \right] |\phi(q)|^2. \quad (8)$$

At this stage, we briefly discuss the dispersion relation of different elastic regimes. The full FLR Hamiltonian is:
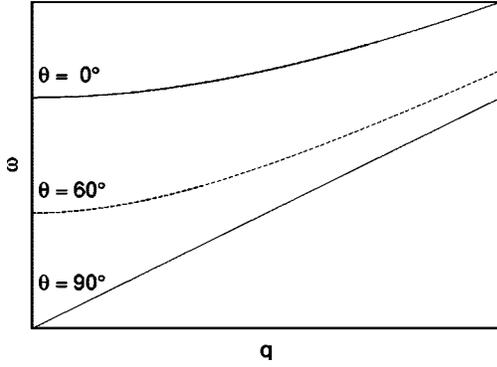
FIG. 1. Dispersion relation of the phase mode given by Eq. (8). The transversal mode ($\theta=90°$) is acoustic, the longitudinal mode is gapped ($\theta=0°$). The gap is reduced by the presence of longitudinal components ($\theta=60°$).

$$H_{\text{FLR}} = \int_{\text{BZ}} \frac{1}{2M} P_q P_{-q} + \frac{c(q)}{2} \phi_q \phi_{-q}, \qquad (9)$$

where P_q is the Fourier transform of the momentum density and M is the phason mass density. The first term gives the kinetic energy and the second the elastic energy. Using the standard canonical transformation we derive the corresponding dispersion relation:

$$\omega(q) = \sqrt{\frac{c(q)}{M}}. \qquad (10)$$

If we decompose the vector q in its longitudinal ($q_x=q\cos\theta$) and transversal ($q_\perp=q\sin\theta$) components, it is clear that in the short-range case q obeys a linear dispersion law, with a slope equal to $\sqrt{[c_1\cos(\theta)+c\sin(\theta)]/M}$. The dispersion for the long-range elasticity (8) is displayed in Fig. 1: The transversal modes remains acoustic, the longitudinal ones instead develop a gap.[24]

Finally, we consider the effect of a distribution of impurities with concentration n_I. The simplest coupling with the electron density is expressed by:

$$H_{\text{dis}} = \pm V_0 \int d^3r \Sigma(r)\rho(r), \qquad (11)$$

where $\Sigma(r)$ is the impurity probability distribution. Long range interactions are neglected and V_0 is a positive constant which measures the impurity potential. At last the sign $+(-)$ is related to the repulsive (attractive) interaction between the electrons and the local impurity. Above two dimensions we can drop out the forward scattering term in the development of $\rho(r)$. In fact, this term leads only to a trivial redefinition of the correlation functions.[11] If V_0 is small (the opposite case, the effect of a strong impurity, is discussed in Ref. 25) the FLR model for the elasticity is justified. In this case, the collective pinning $\Sigma(r)$ is well described by a Gaussian distribution with zero average (we can always incorporate the effect of the averaged disorder into the bare parameters) and the correlator is given by $\overline{\Sigma(r)\Sigma(r')}=N_I\delta(r-r')$, with $N_I=n_I(1-n_I)$. In the following,

we will restrict our analysis to the repulsive case: $\rho_1|\psi|$ is absorbed in V_0 and we define the disorder strength $D=V_0^2 N_I$.

On one hand, the disorder favors local distortions of the phase ϕ, on the other hand these deformations increase the elastic energy. A natural size R_a is defined if we consider the region where ϕ varies by 2π. A simple energetic balance gives for a d-dimensional CDW:

$$E_{\text{tot}} = \frac{c}{2}\left(\frac{2\pi}{R_a}\right)^2 - \frac{D^{1/2}}{R_a^{d/2}}. \qquad (12)$$

Optimizing the gain in potential energy versus the cost in elastic energy we get $R_a=(c^2/D)^{1/(4-d)}$ (for $d=3$ $R_a=c^2/D$). This length, called Fukuyama-Lee length (or Larkin-Ovchinikov length),[15,26] is interpreted as the correlation length of the system. In this scenario the equilibrium state is always disordered and the long-range coherence in the phase is lost. Nevertheless, in this paper we show that, as in the case of vortex lattice, the latter prediction is correct only if we consider scales smaller than R_a, while it breaks down at larger distances. In particular, we see that it is the Fukuyama-Lee length to define the crossover between the short distance regime and the asymptotic one.

III. SPECTRUM INTENSITY

The x-ray diffraction is a powerful tool to detect any subtle change of the perfect crystalline structure. The electron density modulation is accompanied, via the electron–phonon interaction, by a lattice distortion u given by

$$u(r) = \frac{u_0}{Q} \nabla \cos[Qr + \phi(r)] \propto \nabla\rho(r). \qquad (13)$$

Thus, the CDW instability produces a permanent sinusoidal displacement of the atoms from their equilibrium position. This deformation is signaled, in the x-ray spectrum, by the presence of satellite peaks around each principal Bragg peak. The analysis of the shape, the intensity and the symmetry of such peaks allows to fully characterize the structural properties of the CDW. In this section, we isolate the different terms which contribute to the satellite peaks, and study their symmetry properties. This discussion is general and model independent.

The expression for the total diffraction intensity of a crystal is:[27]

$$I(q) = \frac{1}{V}\sum_{i,j} e^{-iq(R_i-R_j)}\langle\overline{f_i f_j e^{-iq(u_i-u_j)}}\rangle. \qquad (14)$$

As shown in Fig. 2, u_i is the atom displacement from the equilibrium position $R_i=ia$, with a indicating the lattice constant. $\overline{\langle\ldots\rangle}$ denotes the double average over the disorder and over the thermal fluctuations. f_i represents the total amplitude scattered by the atom at the position i and depends exclusively on the atom type. We consider the simple case of a disordered crystal, made of one kind of atoms, characterized by the scattering factor f, and containing impurities of scattering factor f_I. To understand the role of the scattering
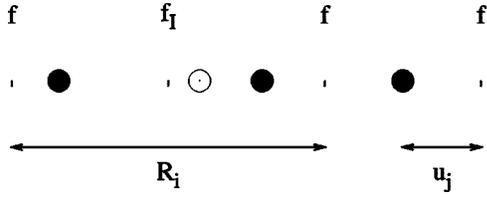
FIG. 2. Example of one-dimensional crystal. The position of the ith atom is given by the equilibrium position R_i and the displacement u_i. In the figure the black circles are the host atoms with scattering factor f and the white circle represents an impurity with scattering factor f_I.

factors, let us start by evaluating the case of fixed atoms ($u_i=0$). We obtain:

$$I(q) = \overline{f}^2 \sum_K \delta(q - K) + \Delta f^2 N_I, \tag{15}$$

where $\Delta f = f_I - f$ and $\overline{f}$ is the average scattering factor. The usual Bragg peaks, corresponding to the reciprocal lattice vectors K, arise from the first term in Eq. (15), while the second term is responsible for a constant background intensity, called Laue scattering, due to the disorder.

Now we move back to the general case $u_i \neq 0$. We are interested in the behavior of the scattering intensity $I(q)$ near a Bragg peak ($q \sim K$). Since $|\delta q| = |q - K| \ll K$, we can take the continuum limit $i \to r$ and obtain from Eq. (14):

$$I(q) = \int_{r_1, r_2} e^{-i\delta q(r_1 - r_2)} \langle \overline{f_{r_1} f_{r_2} e^{-i\delta q[u(r_1) - u(r_2)]}} \rangle, \tag{16}$$

where $\int_{r_1, r_2} = 1/Va^d \int d^d r_1 d^d r_2$ and $f_r = \overline{f} + \Delta f a^{d/2} \Sigma(r)$. Assuming that in the elastic approximation the displacements remain small ($u_i \ll R_i$), one can expand Eq. (16) as a power series of Ku_0. Developing up to the second order we get:[18]

$$I(q) = I_d + I_a + I_{\text{tripl}}, \tag{17}$$

with

$$I_d = \overline{f}^2 q^2 \int_{r_1, r_2} e^{-i\delta q[u(r_1) - u(r_2)]} \overline{\langle u(r_1)u(r_2) \rangle},$$

$$I_a = -iq\Delta f \int_{r_1, r_2} e^{-i\delta q[u(r_1) - u(r_2)]} \overline{\langle \Sigma(r_1)u(r_2) - \Sigma(r_1)u(r_2) \rangle},$$

$$I_{\text{tripl}} = -iq\Delta f^2 a^d \int_{r_1, r_2} e^{-i\delta q[u(r_1) - u(r_2)]}$$
$$\times \overline{\langle \Sigma(r_1)\Sigma(r_2)[u(r_1) - u(r_2)] \rangle}.$$

While the contribution I_d represents the intensity due to the atomic displacements alone, the contributions I_a and I_{tripl} are generated by the coupling between the disorder and the displacements. In the following we consider only I_a and I_d; the term I_{tripl} is evaluated in Appendix A where we show that it is smaller than the other two.

In a pure system [$\Sigma(r) = 0$] we expect that only the first term can be different from zero. Referring to the case of a CDW without disorder and neglecting the thermal fluctuations, we can replace in Eq. (17) the displacement term Eq. (13) with $\phi(r) = \text{const}$. This gives:

$$I_d(q) = f^2 q^2 \sum_K \delta(q \pm Q - K). \tag{18}$$

The presence of two satellites around each Bragg peak is one of the most clear experimental evidence of a CDW. In a pure system these satellites are symmetric and without any broadening. To interpret the experimental findings,[16,17,19] which reveal the presence of asymmetric peaks, we need to account for the effect of impurities. In particular, we want to explain not only the measured intensity asymmetry (IA) between the two satellites, but also the profile asymmetry (PA) of each peak, which is measured in strongly doped samples.

The symmetry properties of the terms I_a and I_d can be determined by considering the lattice displacements and the disorder expressed in terms of their Fourier components:

$$u(r) = \int_{\text{BZ}} e^{-iqr} u_q$$

$$\Sigma(r) = \int_{\text{BZ}} e^{-iqr} \Sigma_q. \tag{19}$$

It is easy to obtain:

$$I_d(q) = \overline{f}^2 q^2 \overline{\langle u_{\delta q} u_{-\delta q} \rangle}, \tag{20}$$

$$I_a(q) = 2a^{d/2} q \Delta f \overline{f} \overline{\langle Im[\Sigma_{-\delta q} u_{\delta q}] \rangle}. \tag{21}$$

The two prefactors, $\overline{f}^2 q^2$ and $\Delta f \overline{f} q$ vary slowly in q and one can assume they are constant in the neighborhood of the reciprocal lattice vector K. Due to the fact that Eq. (21) is an imaginary part, we can deduce:

$$I_d(K + \delta q) = I_d(K - \delta q)$$

$$I_a(K + \delta q) = -I_a(K - \delta q). \tag{22}$$

In Fig. 3 we show the following symmetry properties of different terms: I_d generates two satellites symmetric with respect to the Bragg peak, while I_a gives antisymmetric contributions. We conclude that the IA is due to I_a while the PA is not excluded in both terms, in particular we have a mirror symmetry for I_d. Plugging the displacement form Eq. (13) given by the FLR model in Eq. (20), we get

$$I_d(K + Q + k) = u_0^2 f^2 K^2 \int_r e^{-ikr} C_d(r), \tag{23}$$

where $\int_r = 1/a^d \int d^d r$ and $C_d(r)$ is the positional correlation function

$$C_d(r) = \langle \overline{e^{i[\phi(r/2) - \phi(-r/2)]}} \rangle. \tag{24}$$

Examining this equation one is able to connect the symmetry properties of the satellite peak profile with the symmetry
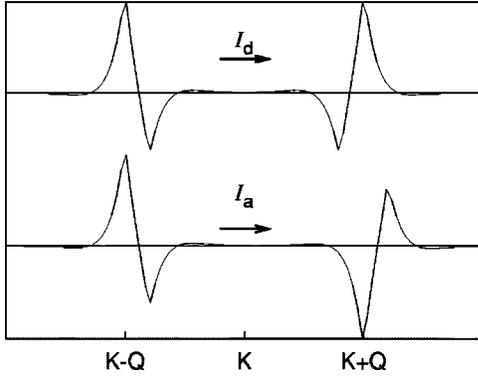
FIG. 3. Sketch showing the symmetry properties of the two different terms contributing to the satellite intensities (the Bragg peak at K is not shown). Top: term I_d. The intensity is symmetric with respect to the Bragg peak. Bottom: term I_a. The intensity is antisymmetric with respect to the Bragg peak.

properties of the system. In particular, if $C_d(r)$ is an even function in r, the I_d term cannot show a PA. On the other hand $I_d(q)$ is a real function so the latter condition is equivalent to require the presence of a $\phi \rightarrow -\phi$ symmetry in the system. We will make use of these observations to interpret the experimental findings in Sec. IV.

IV. THE REPLICA METHOD

In this section we calculate the different terms of the development of Eq. (17) using a Gaussian variational approach.[11,28] We consider first the isotropic case, to include later the corrections due to the Coulombian interactions. The physical interpretation of these results is presented in more detail in Sec. IV.

We consider a FLR Hamiltonian $H = H_{el} + H_{dis}$ where the second term is Eq. (11) and the first one is described either by Eq. (3), in case of a short range elasticity, or by Eq. (8) taking into account the effect of long-range Coulombian interactions. We first perform the average over the disorder using the replica techniques. The replicated Hamiltonian is

$$H_{eff} = \sum_a H_{el}^a - \int d^d r \frac{D}{T} \sum_{a,b} \cos[\phi_a(r) - \phi_b(r)], \quad (25)$$

where T is the temperature and the sum over the n replicas has to be considered in the limit $n \rightarrow 0$. We observe that the system is $\phi \rightarrow -\phi$ invariant. This means that the FLR model with a Gaussian disorder cannot generate satellite peaks with a PA. Finally, we stress that, moving from the original Hamiltonian to its replicated version we also need to change the correlation functions containing explicitly the disorder. In particular, using Eq. (13), the terms I_d and I_a obtained in Eq. (17) become

$$I_d = F_d \int_{r_1, r_2} e^{-i\delta q(r_1 - r_2)} \nabla_{r_1} \nabla_{r_2} \langle \rho_1(r_1) \rho_1(r_2) \rangle_{eff}$$

$$I_a = F_a \int_{r_1, r_2} e^{-i\delta q(r_1 - r_2)} \frac{\nabla_{r_1} - \nabla_{r_2}}{n} \sum_{a,b}^n \langle \rho_a(r_1) \rho_b(r_2) \rangle_{eff},$$

where $F_d = \bar{f}^2 q^2 u_0^2 / Q^2$ and $F_a = iqu_0 D a^{d/2} \Delta f \bar{f} / QTV_0$. Replacing the backward scattering term of the electron density and performing an integration by parts we get to the form:

$$I_d = \bar{f}^2 q^2 u_0^2 \int_r e^{-i\delta q r}[e^{-iQr} + c.c.]C_d(r), \quad (26)$$

$$I_a = -\bar{f}\Delta f qu_0 \sqrt{N_I a^d D} \int_r e^{-i\delta q r}[e^{-iQr} - c.c.]C_a(r).$$

$$C_d(r) = \frac{1}{n} \sum_a \langle e^{i[\phi_a(r/2) - \phi_a(-r/2)]} \rangle_{eff}$$

$$C_a(r) = \frac{1}{Tn} \sum_{a,b}^n \langle e^{i[\phi_a(r/2) - \phi_b(-r/2)]} \rangle_{eff}$$

are the positional correlation functions controlling the behavior of each contribution. To obtain this result we have applied the standard decomposition in center of mass R and relative r coordinates ($r_1 = R + r/2$ and $r_2 = R - r/2$). Since u varies slowly at the scale of the lattice spacing, we performed the integration over R. We notice that Eq. (26) reveals clearly the presence of two peaks situated at $q = Q + K$ and $q = K - Q$. In particular, as expected, the contribution to the two satellites of the displacement term I_d is symmetric, while the one of I_a is antisymmetric. The sum of these two terms leads to the IA experimentally observed.

Following the same method used to study the flux lines in the presence of a weak disorder,[11] we can evaluate the different terms in Eq. (26). We look for the best trial Gaussian Hamiltonian $H_0 = \int_q G_{ab}^{-1}(q)\phi_a(q)\phi_b(-q)$ in the replica space which approximates Eq. (25). The $G_{ab}^{-1}(q)$ is the $n \times n$ variational matrix. Without loss of generality, this matrix can be chosen of the form $G_{ab}^{-1} = cq^2 \delta_{ab} - \sigma_{ab}$. The connected part is defined as $G_c^{-1} = \Sigma_b G_{ab}^{-1}$. By minimization of the variational free energy we derive that G_c is given by the bare elastic propagator. In the isotropic case we write

$$G_c^{-1} = cq^2. \quad (27)$$

For a long range elasticity, in d dimension, it follows:

$$G_c^{-1} = c_1 \frac{q_x^2}{q^{d-1}} + cq^2. \quad (28)$$

Finally, the parameters σ_{ab} are given by:

$$\sigma_{a \neq b} = \frac{D}{T} e^{-B_{ab}(r=0)/2}, \quad (29)$$

where

$$B_{ab}(r) = \langle [\phi_a(r) - \phi_b(0)]^2 \rangle_0 = 2T \int_{BZ} [\tilde{G}(q) - G_{ab}(q)\cos qr]. \tag{30}$$

$\tilde{G}$ is the diagonal element of G_{ab}. In the Gaussian approximation, the positional correlation functions become:

$$C_d(r) = e^{-\tilde{B}(r)/2} \tag{31}$$

$$C_a(r) = \frac{1}{Tn} \sum_{a,b}^n e^{-B_{ab}(r)/2}, \tag{32}$$

where $\tilde{B}$ is the diagonal element of B_{ab}. In order to simplify the notation we write Eq. (32) as $C_a(r) = \chi(r) C_d(r)$. Finally, using Eq. (30), we get:

$$\chi(r) = \frac{1}{nT} \sum_{a,b}^n e^{-T\int_q [\tilde{G}(q) - G_{ab}(q)]\cos qr}. \tag{33}$$

Two general classes of solutions exist for this problem: while the first class preserves the permutation symmetry of the replicas (RS), the second class (RSB) breaks the replica symmetry. It has been shown[11] that the stable solution for $d > 2$ corresponds to the RSB class, while the RS solution remains valid at short distance. In the following we will refer directly to the $d = 3$ case.

A. Replica symmetric solution

We discuss first the RS solution which gives the correct evaluation of the correlation functions at a distance smaller than R_a. Within this Ansatz the matrix G and B are defined by two of their elements: the diagonal values $\tilde{G}$, $\tilde{B}$, and the off-diagonal ones, $B = B_{a \neq b}$ and $G = G_{a \neq b}$. The simple algebra of symmetric matrix yields, for $n = 0$:

$$\tilde{G} = G_c(1 + G_c \sigma_{a \neq b}), \tag{34}$$

$$\tilde{G} - G = G_c, \tag{35}$$

where from Eqs. (4) and (29), we deduce that $\sigma_{a \neq b} \sim D/T \exp(-\phi_T^2/2)$.

We focus first on the short range elasticity. Replacing the form of G_c given in Eq. (27) we easily calculate the displacement

$$\tilde{B}(r) \sim \phi_T^2 + \frac{4r}{3\pi^2 R_a}. \tag{36}$$

The first term take into account the thermal fluctuations and saturates to ϕ_T^2 at a large distance. The second term, due to the disorder, grows with a power law and it is responsible for the exponential decay of the positional correlation functions. To characterize the spectrum it remains to calculate

$$\chi(r) = \frac{1}{T}[1 - e^{-2\pi^2 T/cr}] \sim \frac{2\pi^2}{cr}. \tag{37}$$

We can conclude that in the RS scenario the two positional correlation functions decay exponentially fast, moreover C_a has a power law extra factor.

Before calculating the stable RSB solution, we evaluate the scaling behavior of the same objects in the case of an unscreened Coulombian potential. The only change consists in taking the connected propagator given in Eq. (28) to determine the physical quantities. It is instructive to discuss first the general d-dimensional case. The displacement takes the form

$$\tilde{B}(r) = \int d^{d-1}q \, dq_x \frac{q^{2d-2}}{[c_1 q_x^2 + c q^{d+1}]^2}[1 - \cos(qr)]. \tag{38}$$

A similar integral was discussed in Ref. 29. A general remark is that q_x scales as $q^{(d+1)/2}$. The scaling behavior of these integrals is determined by small q's, for this reason we can neglect the q_x dependence in q. The strong anisotropy along x and y can be studied performing the following substitution:

$$v = xq_x, \quad t = qy$$

$$z = \sqrt{\frac{c}{c_1}} \frac{x}{y^{\frac{d+1}{2}}}. \tag{39}$$

We obtain

$$\tilde{B}(r) = \frac{y^{\frac{9-3d}{2}}}{\sqrt{c^3 c_1}} \int d^{d-1}t \frac{dv}{z} \frac{t^{2d-2}}{\left[\left(\frac{v}{z}\right)^2 + t^{d+1}\right]^2}[1 - \cos(t+v)]$$

$$= \frac{y^{\frac{9-3d}{2}}}{\sqrt{c^3 c_1}} H_1(z), \tag{40}$$

where $H_1(0) = $ const. and $H_1(z \to \infty) \propto z^{(9-3d)/(d+1)}$. It is easy to check that, for $d = 3$, there are only logarithmic divergences:

$$\tilde{B}(x = 0, y) \sim \frac{D}{(2\pi)^2 \sqrt{c^3 c_1}} \log(\Lambda y),$$

$$\tilde{B}(x, y = 0) \sim \frac{D}{2(2\pi)^2 \sqrt{c^3 c_1}} \log(\Lambda_x x).$$

This result is a clear evidence that, because of the long range interactions, the system is more rigid and the critical upper dimension becomes $d = 3$, in contrast with the result $d = 4$ for the short range case. To confirm this statement we evaluate the Fukuyama-Lee length by imposing $\tilde{B}(r) = (2\pi)^2$:

$$\tilde{R}_a(x = 0, y) \sim \Lambda^{-1} e^{\frac{(2\pi)^4 \sqrt{c^3 c_1}}{D}},$$

$$\tilde{R}_a(x, y = 0) \sim \Lambda_x^{-1} e^{\frac{2(2\pi)^4 \sqrt{c^3 c_1}}{D}}. \tag{41}$$

The exponential law is characteristic of the upper critical dimension and is an extrapolation of the power law. The

equivalent form Eq. (B7) has been derived for an isotropic short-range elasticity in $d=4$.[30,31] It remains to determine Eq. (37). At low temperature we write

$$
\chi(r) \sim \int d^d q q^{d-1} \frac{\cos qr}{c_1 q_x^2 + c q^{d+1}}
$$

$$
= \frac{y^{\frac{5-3d}{2}}}{\sqrt{cc_1}} \int d^{d-1}t \frac{dv}{z} \frac{t^{d-1}}{\left(\frac{v}{z}\right)^2 + t^{d+1}} \cos(t+v)
$$

$$
= \frac{y^{\frac{5-3d}{2}}}{\sqrt{cc_1}} H_2(z), \tag{42}
$$

where $H_2(0)=$ const. and $H_2(z \to \infty) \propto z^{(5-3d)/(d+1)}$. In $d=3$ a straightforward calculation confirms this scaling behavior:

$$
\chi(x, y=0) \sim \frac{1}{16 \pi c x}
$$

$$
\chi(x=0, y) \sim \frac{1.1}{2 \pi^2 \sqrt{cc_1} y^2}.
$$

We observe that the anisotropic scaling $x \sim y^2$ is always verified. Since for $d=3$ the RS solution is unstable, to obtain the physics at large distance one has to consider the RSB method.

B. Replica symmetric breaking solution

Within this scheme, the off diagonal elements of $G_{ab}(q)$ are parametrized by $G(q,v)$ where $0 < v < 1$. The saddle point equation becomes

$$
\sigma(v) = \frac{D}{T} e^{\frac{-B(r=0,v)}{2}}. \tag{43}
$$

We look for a solution such that $\sigma(v)$ is constant above a variational breakpoint v_c. This can be done in an easy manner by recasting the equations in terms of a new variable

$$
[\sigma](v) = v\sigma(v) - \int du \sigma(u). \tag{44}
$$

It is not difficult to show that $[\sigma]'(v) = v\sigma'(v)$. We refer to Appendix B, where we summarize the previous results for $[\sigma]$ and we calculate its form in the case of an unscreened Coulombian elasticity. As a first step one uses the inversion rules of hierarchical matrices,[28] Eqs. (34) and (35) become

$$
\widetilde{G} = G_c\left(1 + \int \frac{dv}{v^2} \frac{[\sigma]}{G_c^{-1} + [\sigma]}\right), \tag{45}
$$

$$
\widetilde{G} - G = \left[\frac{1}{G_c^{-1} + \Sigma} + \int\limits_v^{v_c} dt \frac{\sigma'(t)}{[G_c^{-1} + [\sigma](t)]^2}\right], \tag{46}
$$

where $\Sigma = [\sigma](v_c)$ is a variational parameter, whose expression is determined in Appendix B.
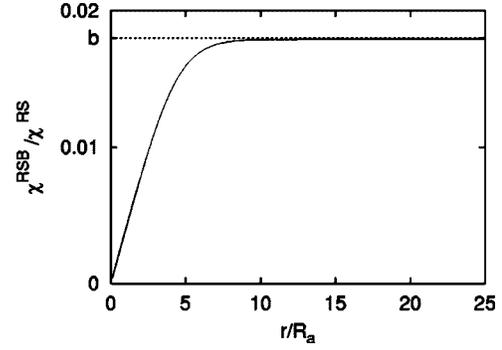
FIG. 4. Ratio between the RSB and RS solutions of $\chi(r)$. At large distance this ratio tends towards a constant value b, with $b \sim 0.018$. This means that the RSB solution affects $\chi(r)$ only by a multiplicative factor.

Starting from the short range case we calculate the displacement using Eq. (45), replacing the expression (B3) for $[\sigma]$:[11]

$$
\widetilde{B}(r) \sim \phi_T^2 + 4\pi^2 \int\limits_{BZ} \frac{[1 - \cos qr]}{q^3} \sim \phi_T^2 + 2\log(\Lambda r). \tag{47}
$$

The logarithmic behavior[9,10] of Eq. (47) is controlled by small $v(v < v_c)$. Values of v above the breaking point ($v > v_c$) give the small distance contribution. To fully characterize the spectrum it still remains to evaluate $\chi(r)$ in the RSB scenario:

$$
\widetilde{G}(q) - G(q,v) \sim \frac{2}{cl^2} \int\limits_{v/v_c}^{1} dt \frac{1}{[q^2 + (t/l)^2]^2}, \tag{48}
$$

where the parameters l and v_c are given by Eq. (B4). By integrating Eq. (48) over q and with some manipulations, we get:

$$
\chi(r) = \frac{v_c}{T}\left[1 - \int\limits_0^1 dz \exp\left(-8\pi^3 \int\limits_z^1 \frac{dt}{t} e^{-rt/l}\right)\right]. \tag{49}
$$

The low temperature behavior ($l \sim R_a$) of this term is sketched in Fig. 4.

Finally we study the RSB solution for the Coulombian elasticity. Replacing Eq. (B8) in Eq. (45), the diagonal correlator becomes

$$
\widetilde{G} \sim G_c \int \frac{dv}{v} \frac{1}{G_c^{-1}\log^2\left(\frac{A_{lr}v}{\sqrt{c_1 c}\Lambda_x}\right) + A_{lr}v}
$$

$$
\sim G_c^2 \log^{-1}\left(\frac{G_c^{-1}}{\sqrt{c_1 c}\Lambda_x}\right). \tag{50}
$$

The latter form is characteristic of the upper critical dimension. Inserting Eq. (50) in Eq. (30), taking $c_1 = c = 1$, and employing the usual substitution Eq. (39) we get
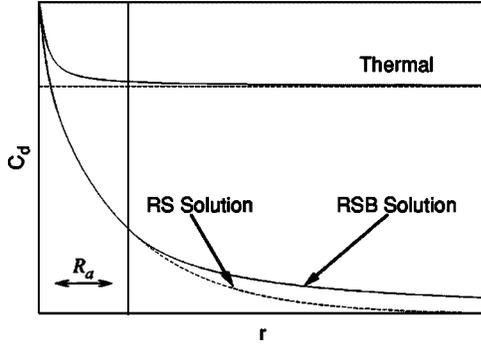
FIG. 5. Behavior of $C_d(r)$. The thermal contribution saturates to $\exp(-\phi_T^2/2)$, the RSB solution is valid beyond R_a, while the RS one is valid below R_a.

$$\widetilde{B}(r) = S_2 \int dt \frac{dv}{z} \frac{t^5}{\left[\left(\frac{v}{z}\right)^2 + t^4\right]^2} [1 - \cos(t+v)].$$

This equation leads to the same conclusions discussed for the isotropic upper critical dimension. The asymptotic displacement is thus given by

$$\widetilde{B}(x) \sim \log[\log(\Lambda_x x)]. \tag{51}$$

As in the case of the short-range elasticity, it can be shown that the RSB solution does not affect the asymptotic power low behavior of $\chi(r)$.

V. PHYSICAL DISCUSSION

In this section we summarize the results obtained in the previous sections and compare them with the experimental findings.

We start by evaluating for the short-range elasticity model the positional correlation function $C_d(r)$, defined in Eq. (24). This function is the analog of the correlation function determined for vortex line systems.[11] It is well known that for $d > 2$ it exists a finite temperature (the critical temperature T_c) below which thermal fluctuations are prevented from disordering the system. In fact, the direct calculation of the positional correlation function in $d=3$ yields

$$C_d^{\text{therm.}}(r) = e^{\frac{\phi_T^2}{2}[1 - \text{S}i(\Lambda r)/\Lambda r]}, \tag{52}$$

with $\text{S}i(\Lambda r) = \int_0^{\Lambda r} dt \sin t / t$. As shown in Fig. 5 the correlation function saturates after a few lattice parameters to a nonzero value, which witnesses the presence of long-range order in the system.

However, the quenched noise originated in the impurities is still able to destroy the long range order, even in $d=3$ (see Fig. 5). In this circumstance, the more traditional scheme[32] describes the system as organized in ordered domains (called Fukuyama-Lee-Rice domains), characterized by the average size R_a. Beyond this characteristic length, the CDW dislocations become dominant and any order disappears. This scenario is captured by the RS solution. From Eq. (36) we obtain:

$$C_d^{\text{RS}}(r) = C_d^{\text{therm.}}(r) e^{-\frac{4r}{3\pi^2 R_a}}. \tag{53}$$

As a direct consequence, we expect to find Lorentzian satellites, whose half-width at half-height is of the order of R_a^{-1}. However, the RS approach is unstable at large distances and the correct solution is given asymptotically by the RSB. Within this assumption, the correlations decrease following a power law:

$$C_d^{\text{RSB}}(r) = C_d^{\text{therm.}}(r) e^{-\frac{4}{3\pi^2}\left(\frac{R_a}{r}\right)^\eta}. \tag{54}$$

Applying the variational approach,[33] one finds, from Eq. (47), $\eta = 1$. The corresponding quasi-ordered phase,[11,10] called Bragg glass, is characterized by an infinite correlation length and the characteristic size R_a represents now the crossover between the RS and RSB solutions. One can give a simple physical interpretation of the two identified regimes, by observing that at the scale R_a the phase distortions are of the order of the CDW period 2π. This means that for distances smaller than R_a the development of the Hamiltonian Eq. (25) is allowed and leads to the RS solution. For distances larger than R_a, instead, the phase feels its periodic nature and this trivial development of the Hamiltonian is no more valid.

In order to determine the intensity and the shape of the two satellites we need to evaluate all the terms contributing to the development Eq. (17). In particular, we consider the displacement term I_d, and the asymmetric term I_a, arising from the coupling between disorder and displacement. In the literature this latter term was previously estimated by means of models[17–19] which describe the pinning imposing a constant value ϕ_0 on the phase in proximity of each impurity. According to these approaches, the observed satellite asymmetry is a clear signature of strong disorder.[17] Thanks to our more accurate calculation, we found that the term I_a is nonzero also in case of weak disorder and it gives rise to a divergent contribution similar to the one stemming from I_d. Using Eqs. (37), (47), and (49), our final results read:

$$I_d(K+Q+k) = \overline{f}^2 K^2 u_0^2 \int_r e^{-ikr} \left(\frac{R_a}{r}\right)^\eta, \tag{55}$$

$$I_a(K+Q+k) = -2\pi^2 \overline{f} \Delta f \sqrt{\frac{N_I a}{R_a}} K u_0 \int_r e^{-ikr} \left(\frac{R_a}{r}\right)^\eta \frac{ba}{r}.$$

After computing the d-dimensional Fourier transforms, we conclude that both terms are divergent: in particular, $I_d \propto 1/q^{d-\eta}$ and $I_a \propto 1/q^{d-\eta-1}$. This result, summarized in Fig. 6, is a clear sign of the quasi-long range positional ordered phase. In this particular case, the peak at $K+Q$ is smaller than the $K-Q$ one, since the specific interaction between the impurity and the CDW is repulsive (we would have the opposite asymmetry in case of an attractive interaction). We observe that for an ideal experiment with infinite resolution the symmetric term would be dominant, as $C_d(r)$ decays to zero less rapidly than $C_a(r)$. However, in a real measurement
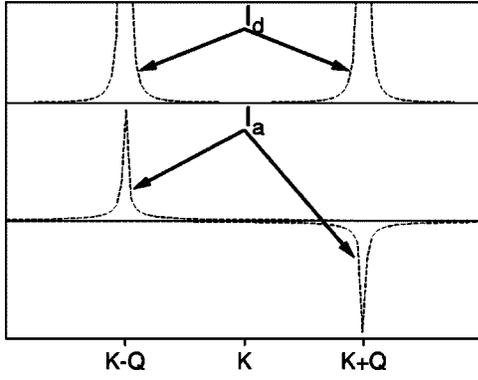
FIG. 6. Intensities of the different contributions to satellite peaks. The more divergent term, I_d, is symmetric. I_a is antisymmetric. In this figure we consider a repulsive potential and $\Delta f > 0$.

the divergence in Eq. (55) is always cut by the finite resolution and both terms have to be accounted for, as the prefactor Ku_0 of the less divergent term I_a is larger.

At this stage, following the analysis of the experimental data of Ref. 14 concerning neutron diffraction spectra, it is interesting to discuss the role played by the experimental resolution in determining the peak shape. With the low resolution achieved by means of neutrons to describe a vortex lattice, in the above cited experiment,[14] it is possible to determinate the intensity spectrum only along one direction, after performing an integration on the other two directions. Instead, the much higher resolution reachable in x-rays experiments, is in principle adequate to perform the whole three-dimensional Fourier transform of the spectrum. For concreteness sake, we assume a Gaussian resolution with variance ξ^2, where $\xi > R_a$ (the opposite case is not interesting as the resulting peak shape is affected only by the resolution). We consider first the behavior of the direct term I_d in case of a RS solution. The peak obtained from the $C_d^{RS}(r)$ function is essentially independent of the resolution and has the shape of as a squared Lorentzian of height $\propto R_a^3$ and half-width $\propto 1/R_a$. The profile drastically change if we consider instead the correct RSB solution. Setting $\eta = 1$ we can find an analytical expression for the experimental peak:

$$I_d^{\exp}(K+Q+k) \propto R_a^2 \int_r e^{-ikr} e^{-r^2/2\xi^2} \frac{1}{r}$$

$$= (2\pi)^{3/2} \frac{R_a^2 \xi}{k} e^{-k^2\xi^2/2} \operatorname{erf} i\left(\frac{k\xi}{\sqrt{2}}\right), \quad (56)$$

where $\operatorname{erf} i(x) = -i \operatorname{erf}(ix)$ is the imaginary part of the error function. This expression gives a nondivergent peak, shown in Fig. 7, whose height is $4\pi \bar{f}^2 K^2 u_0^2 R_a^2 \xi^2$ and its half-width $\sim 1.5034/\xi$. We remark that the peak decays with the characteristic law q^{-2} only for $R_a^{-1} < q \ll \xi^{-1}$, while a wide region around the maximum height is dominated by the effects related to the finite resolution. In Fig. 7 we also report the function $I_d^{\text{approx}}(q) = I_d^{\exp}(0)(1 - q^2\xi^2/3)$. It is possible that, in a real experiment, the signal–noise ratio is low enough to hide the q^{-2} behavior. In this specific case, to put in evidence the
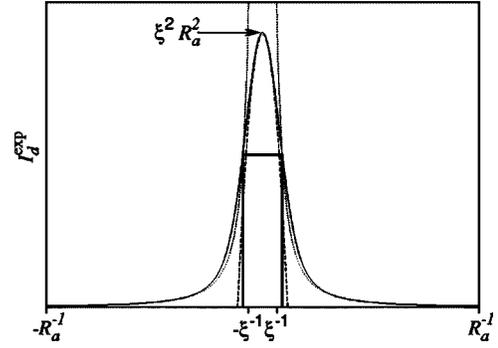
FIG. 7. Dotted line: divergent peak $I_d(q) = q^{-2}$ for a perfect experimental resolution. Full line: peak convolved with a finite experimental resolution according to Eq. (56). The height of the peak is $\sim \xi^2 R_a^2$, the half-width half-height $\sim \xi^{-1}$ is also indicated. Dashed line: an approximate form for the peak $I_d^{\text{approx}}(q) = I_d^{\exp}d(0) \times (1 - q^2\xi^2/3)$.

existence of a Bragg glass regime one should vary the Fukuyama-Lee length R_a.[14] In fact, if the peak shape is Lorentzian, varying R_a produces a change both in the width and the height of the peak, whereas if the peak follows a power law, only its height is changed due to a variation of R_a, while the width is fixed by the resolution.

In absence of screening, the long range Coulomb interactions become important: the system is more rigid and the upper critical dimension is shifted from $d=4$ to $d=3$. As a consequence, the satellite peaks become more divergent. In particular, we find that the symmetric term I_d goes asymptotically as q^{-3} instead of q^{-2}. Moreover, the strong anisotropy between the longitudinal direction (x) and the transversal ones (y) leads to an anisotropic scaling of the correlation functions. We verified that in $d=3$ the dependence on x and y of the correlation functions [as clearly shown in Eq. (42)] and of the characteristic length scale Eq. (41) respects the relation $f(x,y=0) \sim f(x=0,y^2)$. As a result, in this regime, we expect more divergent and more anisotropic peak shapes in comparison to the ones observed in the short-range case.

On the experimental side few detailed diffraction spectra are available at the moment. An example of prototype systems are doped blue bronzes,[16] where the disorder is intro-
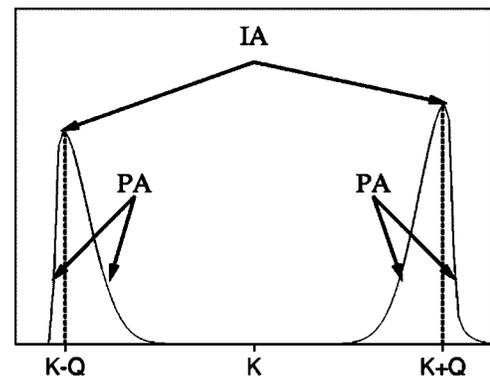
FIG. 8. Sketch of the experimental findings (Ref. 16). The two satellites present an IA in agreement with our predictions, but also an evident PA.

duced by partially replacing Mo^{6+} for the nonisoelectric V^{5+}. In this kind of system, the interactions between the CDW and the impurities are repulsive and Δf is negative. The shape of the observed spectrum is sketched in Fig. 8. The sign of IA is consistent with our prediction as well as with the predictions of the strong pinning approach. However, we also remark the presence of PA of each single satellite. The mirror symmetry of the shape of the two peaks suggests that the PA is originated in the correlation function $C_d(r)$. As we have previously discussed, the correlation function obtained from the FLR model with Gaussian disorder is real and produces two peaks with profile symmetry. One can wonder what is the effect of non-Gaussian disorder. To this purpose, we studied a one-dimensional model with a binomial distribution of impurities. If we restrict to the forward scattering term in the development (1), the problem is exactly soluble. We find two Lorentzian peaks without PA, centered around a vector $K \pm \tilde{Q}$ shifted with respect to $K \pm Q$ as a consequence of the presence of odd moments in the disorder distribution. It remains to investigate the role possibly played by the amplitude fluctuations. The short correlation lengths extracted from the experimental data suggest that this particular effect is most likely to happen in the strong pinning regime, whereas our calculations concern the weak pinning limit. The authors of Ref. 16 indeed justify the PA with the presence of Friedel oscillations and hence with the presence strong fluctuations of the amplitude of the condensate, at least in the neighborhood of the impurities.

VI. CONCLUSIONS

Summarizing, we determined the shape and the intensity of the satellite peaks characterizing the spectrum of a pinned charge density wave. We analyzed in detail the case of a weak and collective disorder, when the Fukuyama-Lee-Rice model is justified. We considered both the short-range elasticity as well as the long-range elasticity generated by an unscreened Coulomb interaction. In both these cases, we found divergent peaks displaying intensity asymmetry. The divergent nature of the peaks is, as it was discussed, the clearest sign of a Bragg glass phase. Moreover, the long-range elasticity, when present, is responsible for a larger anisotropy and a stronger divergence. Let us stress that the calculated sign of the intensity asymmetry is in agreement with the experimental data. We discussed the role played by the finite resolution of the experimental setup, calculating the convolved shape of the peaks, where the divergence is cut. From these observations, we illustrated possible methods to reveal experimentally the presence of the Bragg glass phase. Concerning the asymmetry of the peak profile, we showed that, on general symmetry grounds, it is not expected in the weak pinning regime. We conjectured that its observation in a recent experiment[16] is likely due to the strong pinning present in the measured system. Finally, we observe that the profile asymmetry may hide the power law behavior of the satellite peaks. It would thus be highly desirable to dispose of measures in less disordered systems where one can expect a Bragg glass behavior, e.g., using isoelectric impurities.

APPENDIX A: THE TRIPLET TERM

In this appendix we discuss the behavior of the term I_{tripl} of the intensity development (17). This term was only conjectured to be negligible,[18,34] before that[20] a direct calculation of it was performed.

We start analyzing the symmetry properties of I_{tripl} showing it has the same symmetry of I_a. Next we evaluate I_{tripl} within the RS scheme. Independently of the elasticity range, we find that the difference between the two contributions is given by a simple q-independent multiplicative factor.

Applying a Fourier transform (19) we obtain

$$I_{\text{tripl}}(K + \delta q) = -2iK\Delta f^2 a^d \int_{\text{BZ}} \overline{\langle \Sigma_{\delta q} \Sigma_{q_1} u_{-\delta q - q_1} \rangle}. \quad \text{(A1)}$$

This equation gives a nonzero contribution only if we consider higher harmonic terms of the electron density (1): $\rho(x) \sim \rho_1 |\psi| \cos\{Q[x + \phi(x)]\} + \rho_1 |\psi| \cos\{2Q[x + \phi(x)]\}$. The two satellites take the form:

$$I_{\text{tripl}}(K + \delta q) = -2iK\Delta f^2 a^d \overline{\langle \Sigma_{\delta q}[\Sigma_{-2\delta q} u_{\delta q} + \Sigma_{\delta q} u_{-2\delta q}] \rangle}.$$

At this stage it is evident that I_{tripl} has the same symmetry of I_a. Performing the integration over the Gaussian disorder by means of the standard replica techniques we obtain

$$I_{\text{tripl}} = \Delta f^2 q u_0 N_I a^d D \int_r e^{-i\delta q r}[e^{-iQr} - \text{c.c.}]C_{\text{tripl}}(r).$$

Using the usual decomposition $C_{\text{tripl}}(r) = e^{-\tilde{B}/2}\chi_{\text{tripl}}(r)$ we write

$$\chi_{\text{tripl}}(r) = \frac{1}{nT^2}\sum_{a,b,c}[e^{-T\int_{\text{BZ}}2[\tilde{G}-G_{ac}]}e^{-T\int_{\text{BZ}}[(\tilde{G}-G_{ab})+(G_{bc}-G_{ab})]\cos qr}].$$

$$\text{(A2)}$$

We introduce the replica symmetric Ansatz. It is easy to check that for $n = 0$

$$\frac{1}{n}\sum_{abc}A_{abc} = A_{aaa} - \sum_{a \neq b}(A_{aab} + A_{aba} + A_{baa}) + 2\sum_{a \neq b \neq c}A_{abc}.$$

Using this relation and Eq. (35) we can evaluate $\chi_{\text{tripl}}(r)$. In order to simplify the notation we recall that $\phi_T^2 = 2T\int_{\text{BZ}}G_c$ and $\chi(r) = [1 - \exp(-T\int_{\text{BZ}}G_c \cos qr)]/T$. From Eq. (A2) we obtain

$$\chi_{\text{tripl}}(r) = \frac{\chi(r)}{T}\left\{1 - e^{-\phi_T^2/2}\left[2\sinh\left(T\int_{\text{BZ}}G_c\cos qr\right) + 1\right]\right\}.$$

Because we are interested in the long distance behavior we remark that $\int_{\text{BZ}}G_c \cos qr \to 0$, whenever $r \to \infty$. Developing up to the first order we get
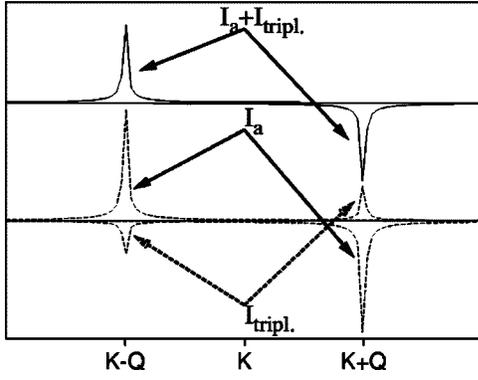
FIG. 9. Intensities of the antisymmetric contributions to satellite peaks. We remark that $I_a \gg I_{\text{tripl}}$.

$$\chi_{\text{tripl}}(r) \sim \chi(r) \frac{1 - e^{-\phi_T^2/2}}{T} \sim \chi(r) \frac{\phi_T^2}{2T}, \tag{A3}$$

where the last step is valid at low temperature. In fact, in this regime $C_{\text{tripl}}(r)$ and $C_a(r)$ have the same behavior in r. If we take a spherical cutoff $\Lambda = 2\pi/a$, where a is the lattice space, the integral $\phi_T^2/(2T) = (c\pi a)^{-1}$ is independent of the range of the elasticity (for $a \to 0$). We can compare the two terms I_{tripl} and I_a, by writing the ratio between the two intensities

$$\frac{I_{\text{tripl}}}{I_a} = -\frac{\Delta f}{\pi \bar{f}} \sqrt{\frac{N_I a}{R_a}}. \tag{A4}$$

For weak disorder $R_a \gg a$; it follows that $I_a \gg I_{\text{tripl}}$.

The evaluation of this term in a more accurate RSB approach is very complicate because $\chi_{\text{tripl}}(r)$ involves the sum over three replicas. However, in analogy with $\chi(r)$ we can argue that the RSB solution does not affect the asymptotic power low behavior of $\chi_{\text{tripl}}(r)$. In Fig. 9 we summarize our result taking the correct RSB behavior for $\tilde{B}$.

We conclude that the triplet term renormalizes the prefactor of I_a without changing the power law behavior. In particular, when $\Delta f > 0$, I_{tripl} enhances the asymmetry between the two satellites, while when $\Delta f < 0$, I_{tripl} slightly decreases the antisymmetric contribution.

APPENDIX B: CALCULATION OF [σ]

In this Appendix we determine the variational function $[\sigma](v)$ defined in Eq. (44). We start from the saddle point Eq. (43). From Eq. (30) we know that

$$B(r = 0, v) = \int_{\text{BZ}} \tilde{G}(q) - G(q, v). \tag{B1}$$

The integral in the momentum space is performed in the Brillouin zone. To simplify the analytical form of our integrals the ultraviolet cutoff, Λ, is taken equal to infinity whenever it is possible (i.e., whenever the integrals are ultraviolet convergent). Inserting Eq. (46) in the previous equation and taking the derivative of Eq. (43) leads to the equation determining $[\sigma]$:
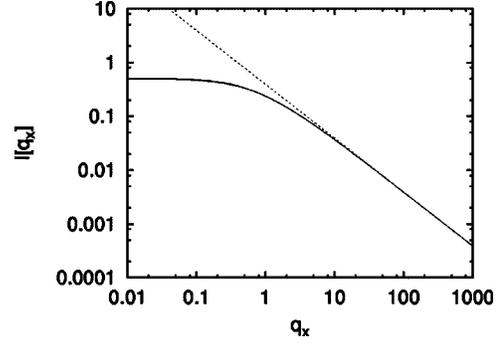
FIG. 10. Continuum line: integral over q in (B8) as a function of q_x. Dotted line: limiting behavior $I[q_x] \to \pi/8q_x$. Finally $I[0] = 0.5$.

$$\sigma(v) \int \frac{d^d q}{(2\pi)^d} \frac{T}{[G_c^{-1} + [\sigma]]^2} = 1. \tag{B2}$$

Solving the integral for $2 < d < 4$ ($\Lambda \to \infty$) and deriving again, one gets

$$[\sigma](v) = \Sigma (v/v_c)^{2/\theta} \quad \text{for } v < v_c$$

$$[\sigma](v) = \Sigma \quad \text{for } v > v_c, \tag{B3}$$

where $\theta = 2 - d$. The values of the breakpoint v_c and $\Sigma = cl^{-2}$ determine the crossover between a short distance regime ($x \ll l$), where $[\sigma]$ is constant and the RS solution valid, and the asymptotic regime ($x > l$), where the physics is determined by the small v behavior of $[\sigma]$. Using Eqs. (B2) and (43), after some manipulation it is found[11] for $d = 3$:

$$l = \frac{1}{8\pi} R_a e^{-\phi_T^2}$$

$$v_c = \frac{T}{8lc}. \tag{B4}$$

We observe that the crossover between the two regimes is $l \sim R_a$ in agreement with the dimensional result in Eq. (12).

For $d = 4$, and more in general at the upper critical dimension, the integral in Eq. (B2) has a logarithmic ultraviolet divergence. As discussed in Ref. 30, the behavior of $[\sigma]$ when v is small is not described by a pure power law. Starting from Eq. (B2) for $d = 4$ we get

$$1 = \sigma(v) \int \frac{d^4 q}{(2\pi)^4} \frac{T}{[cq^2 + [\sigma]]^2}$$

$$= \frac{S_4 \sigma(v) Q^2}{c^2} \int_0^{\sqrt{c/[\sigma]}\Lambda} \frac{q^3 dq}{[q^2 + 1]^2} \sim \frac{S_4 \sigma(v) T}{2c^2} \log\left(\frac{c\Lambda^2}{[\sigma]}\right), \tag{B5}$$

where $S_d = 2^{1-d} \pi^{-d/2}/\Gamma(d/2)$ is the angular integration in d dimension. Defining $A = 2c^2/(S_4 T)$, we obtain after one more derivative

$$[\sigma] = \frac{Av}{\log^2 \frac{[\sigma]}{c\Lambda^2}} \sim \frac{Av}{\log^2 \frac{Av}{c\Lambda^2}}. \tag{B6}$$

This result is valid up to log-log corrections. From Eqs. (B5) and (43) we can estimate the crossover length l. In the short distance regime, where $[\sigma] = cl^{-2}$, it turns out:

$$l \sim \Lambda^{-1} e^{8\pi^2 c^2 / D}. \tag{B7}$$

At this stage we can discuss the case of the Coulombian long range elasticity. Starting from Eq. (B2) and using Eq. (28) for G_c, we write

$$1 = \sigma(v) \int_0^{\Lambda_x} \frac{dq_x}{2\pi} \int_0^\Lambda \frac{d^2q}{(2\pi)^2} \frac{T}{\left[\frac{c_1 q_x^2 + cq^4}{q^2} + (\sigma)\right]^2}.$$

To solve this equation we consider the physical case, where $\Lambda_x \sim Q$, $\Lambda \sim 2\pi/a$ and a is the lattice space. In this limit $\Lambda_x \ll \Lambda$ so we can assume $\Lambda \to \infty$ and solve the integral

$$1 = \frac{T\sigma(v)}{4\pi^2\sqrt{c^3 c_1}} \int_0^{\sqrt{c_1 c}\Lambda_x/[\sigma]} dq_x I[q_x]$$

$$I[q_x] = \int_0^\infty \frac{q^5 dq}{(q_x^2 + q^4 + 1)^2}.$$

The behavior of $I[q_x]$ is shown in Fig. 10. In conclusion, we obtain

$$[\sigma] = \frac{A_{lr}v}{\log^2 \frac{[\sigma]}{\sqrt{c_1 c}\Lambda_x}} \sim \frac{A_{lr}v}{\log^2 \frac{A_{lr}v}{\sqrt{c_1 c}\Lambda_x}}, \tag{B8}$$

where $A_{lr} = 16\pi\sqrt{c^3 c_1}/T$. This equation is equivalent to the one found for an isotropic system at the upper critical dimension.

[1] S. Lemerle, J. Ferré, C. Chappert, V. Mathet, T. Giamarchi, and P. Le Doussal, Phys. Rev. Lett. **80**, 849 (1998).

[2] T. Tybell, P. Paruch, T. Giamarchi, and J. M. Triscone, Phys. Rev. Lett. **89**, 097601 (2002).

[3] S. Moulinet, A. Rosso, W. Krauth, and E. Rolley, Phys. Rev. E **69**, 035103(R) (2004).

[4] E. Bouchaud, J. P. Bouchaud, D. S. Fisher, S. Ramanathan, and J. R. Rice, J. Mech. Phys. Solids **50**, 1703 (2002).

[5] G. Grüner, Rev. Mod. Phys. **60**, 1129 (1988).

[6] G. Blatter, M. V. Feigel'man, V. B. Geshkenbein, A. I. Larkin, and V. M. Vinokur, Rev. Mod. Phys. **66**, 1125 (1994).

[7] R. Chitra, T. Giamarchi, and P. Le Doussal, Phys. Rev. B **65**, 035312 (2001).

[8] T. Nattermann, Phys. Rev. Lett. **64**, 2454 (1990).

[9] S. E. Korshunov, Phys. Rev. B **48**, 3969 (1993).

[10] T. Giamarchi and P. Le Doussal, Phys. Rev. Lett. **72**, 1530 (1994).

[11] T. Giamarchi and P. Le Doussal, Phys. Rev. B **52**, 1242 (1995).

[12] T. Nattermann and S. Scheidl, Adv. Phys. **49**, 607 (2000).

[13] T. Giamarchi and S. Bhattacharya, in *High Magnetic Fields: Applications in Condensed Matter Physics and Spectroscopy*, edited by C. Berthier, L. P. Lévy, and G. Martinez (Springer, Berlin, 2002), p. 314, cond-mat/0111052.

[14] T. Klein, I. Joumard, S. Blanchard, J. Marcus, R. Cubitt, T. Giamarchi, and P. L. Doussal, Nature (London) **413**, 404 (2001).

[15] H. Fukuyama and P. A. Lee, Phys. Rev. B **17**, 535 (1978).

[16] S. Rouzière, S. Ravy, J.-P. Pouget, and S. Brazovskii, Phys. Rev. B **62**, R16 231 (2000).

[17] S. Ravy and J.-P. Pouget, J. Phys. IV **3**, 109 (1993).

[18] S. Ravy, J.-P. Pouget, and R. Comès, J. Phys. I **2**, 1173 (1992).

[19] S. Brazovskii, J.-P. Pouget, S. Ravy, and S. Rouzière, Phys. Rev. B **55**, 3426 (1997).

[20] A. Rosso and T. Giamarchi, Phys. Rev. B **68**, 140201(R) (2003).

[21] S. Brazovskii and T. Nattermann, Adv. Phys. (to be published).

[22] P. A. Lee and H. Fukuyama, Phys. Rev. B **17**, 542 (1978).

[23] P. A. Lee and T. M. Rice, Phys. Rev. B **19**, 3970 (1979).

[24] G. Grüner, *Density Waves in Solids* (Addison-Wesley, Reading, MA, 1994).

[25] I. Tüttő and A. Zawadowski, Phys. Rev. B **32**, 2449 (1985).

[26] A. I. Larkin and Y. N. Ovchinnikov, J. Low Temp. Phys. **34**, 409 (1979).

[27] A. Guiner, *X-Ray Diffraction, Imperfect Crystals and Amorphous Bodies* (W. H. Freeman, San Francisco, 1969).

[28] M. Mézard and G. Parisi, J. Phys. I **1**, 809 (1991).

[29] P. Le Doussal and T. Giamarchi, Phys. Rev. B **57**, 11 356 (1998).

[30] R. Chitra, T. Giamarchi, and P. Le Doussal, Phys. Rev. B **59**, 4058 (1999).

[31] H. Bucheli, O. S. Wagner, V. B. Geshkenbein, A. I. Larkin, and G. Blatter, Phys. Rev. B **57**, 7642 (1998).

[32] K. B. Efetov and A. I. Larkin, Sov. Phys. JETP **45**, 1236 (1977).

[33] For a CDW the elastic object (the phase ϕ) is a scalar. The exponent η is universal and the best prediction is given by FRG calculation $\eta \sim 1.1$. However, also in the case where the elastic object has many components (i.e., for the vortex lattice) the possible variation of this exponent is still less than a percent; [S. Bogner, T. Emig, and T. Nattermann, Phys. Rev. B **63**, 174501 (2001)].

[34] J. M. Cowley, Surf. Sci. **298**, 336 (1993).

[35] In the anisotropic case, for a more realistic description of the system, we introduce two cutoff wave vectors. One, along the Q direction, remains of the order of Q. The others, along the transversal directions, are given by the periodicity of the lattice $\Lambda = \pi/a$.